Supercapacitor Performance of Fe3O4 and Fe3O4@SiO2- bis(aminopyridine)-Cu Hybrid Nanocomposite

Article *in* International Journal of Electrochemical Science · September 2022

CITATION
1

READS
43

10 authors, including:

Mohammed Ahmed
University of Samarra
24 PUBLICATIONS **34** CITATIONS
SEE PROFILE

Qutaiba A. Qasim
University of Basrah
32 PUBLICATIONS **29** CITATIONS
SEE PROFILE

Ahmed B. Mahdi
Al-Mustaqbal University College
23 PUBLICATIONS **36** CITATIONS
SEE PROFILE

Emad Salaam Abood
Hilla university college
44 PUBLICATIONS **138** CITATIONS
SEE PROFILE

Int. J. Electrochem. Sci., 17 **(2022)** Article Number: 221057, doi: 10.20964/2022.10.49

International Journal of
ELECTROCHEMICAL
SCIENCE
www.electrochemsci.org

Supercapacitor Performance of Fe_3O_4 and Fe_3O_4@SiO_2-bis(aminopyridine)-Cu Hybrid Nanocomposite

Mohammed Ahmed Mustafa[1], Qutaiba A. Qasim[2], Ahmed B. Mahdi[3], Samar Emad Izzat[4], Yasir S. Alnassar[5], Emad Salaam Abood[6], Zahara Jalil alhakim[7], Zaid H. Mahmoud[8], Ahmed Mahdi Rheima[9,10] and H.N.K. Al-Salman[11]

[1] Department of medical Laboratory technology, Imam Jaafar Al-Sadiq university,
[2] Al-Ayen university, college of pharmacy, Dhi Qar, IRAQ,
[3] Anesthesia Techniques Department, Al-Mustaqbal University College, Babylon, Iraq,
[4] Al-Nisour University College/Baghdad/Iraq,
[5] The University of Mashreq/ Baghdad/ Iraq,
[6] Medical physics department, Hilla university college, Babylon, Iraq
[7] Department of Nursing, Altossi university college, Najaf,
[8] Diyala university, college of science, chemistry department, Iraq,
[9] Mustansiriyah university, college of science, chemistry,
[10] Dijlah university college, Al-Masafi street, Al-Dora, Baghdad,
[11] university of Basrah, college of pharmacy, Iraq.
*E-mail: Zaidhammed_91@yahoo.com

Received: 25 July 2022 / *Accepted:* 25 August 2022 / *Published:* 10 September 2022

In this study, photolysis and immobilization of bis(aminopyridine)-Cu on the surface of SiO_2-coated Fe_3O_4 nanoparticles were used to create core-shell composites of magnetite (Fe_3O_4) and Fe_3O_4@SiO2-bis(aminopyridine)-Cu. FTIR, ICP-AES, XRD, XPS, FESEM-EDS-mapping, and TEM were used to identify the structural characteristics of the catalyst. TGA was used to test the prepared materials' thermal stability, and CV, GCD, and EIS were used to assess their electrochemical characteristics. The successful shelling of SiO_2 around Fe_3O_4 with a size of 20 nm was confirmed by the TEM images. The results of the electrochemical tests demonstrate that the performance of the synthetic materials is typical for supercapacitors. The shell of SiO_2-bis(aminopyridine)-Cu can boost Fe_3O_4's reversibility and storage energy. After 1000 cycles at 5 A/g, the Fe_3O_4. The Fe_3O_4@SiO_2-bis(aminopyridine)-Cu electrode exhibits good specific capacitance of 265 F/g and excellent cyclic stability with a retention ratio of 85% compared to pure magnetite's 67 percent.

Keywords: hybrid nanocomposite, supercapacitor, photolysis, Fe_3O_4, core-shell

1. INTRODUCTION

Since they have a higher energy density, more power, and a longer cycle life than Li-ion batteries and conventional dielectric capacitors, supercapacitors are regarded as lucky picks for the

development of future power instruments [1-3]. Pseudocapacitors and electrochemical double layer capacitors are two categories of supercapacitor device that can be separated based on the mechanism that determines capacitance (EDLC). The capacitance of pseudocapacitors is related to the redox process (faradic reactions) on the surface of electrodes, such as conductive polymers and oxide nanocomposite, which have a greater capacity for energy storage than materials based on carbon [4,5]. The fast, reversible oxidation-reduction reaction on the surface is used with oxide materials to produce high power and energy densities [6]. Because of its high electric conductivity and specific capacitance of $720Fg^{-1}$, RuO_2 is regarded as one of the most promising oxides for use as an electrode in capacitor applications [7]. However, due to its rarity and high cost, it is only occasionally used in practice applications. As a result, the main focus for these applications shifts to using the less expensive oxides with good energy storage. Due to its abundance, simplicity in preparation, variety of state valance (+2, +3), ability to perform reversible redox reactions, low cost, and environmental compatibility, magnetite (Fe_3O_4) is regarded as an excellent alternative material in this regard [8,9]. The magnetite has drawn the interest of numerous researchers in this field, and they have reported successes with it. Octadecahedron Fe_3O_4 prepared hydrothermally was used by Hung [10] and demonstrated 118 F/g at 6 mA in 1M Na_2SO_3 electrolyte solution. Fe_3O_4 was synthesized by Brousse, who used it as an electrode with a 75 F/g specific capacitance [11]. However, because the kinetics of redox are constrained by electron transfer and mass diffusion, this type of oxide has a shorter cycle life and performs less well during cycles. Researchers' attention was drawn to hybrid nanocomposite supercapacitors because of their high voltage, long cyclic life, and high energy density [12,13]. These capacitors perform well in the field of energy storage. Graphene oxide/metal oxides [14], graphene oxide/metal sulfide [15], and oxides/conducting polymers [16] are examples of composite supercapacitors. It displayed higher specific capacitance in comparison to Fe_3O_4 supercapatiors. We discussed the electrochemical behavior of Fe_3O_4 with a SiO_2 coating and a copper complex as a core-shell system in this work. Numerous studies had claimed [17,18] that Fe_3O_4@SiO_2 and higher values of specific capacitance did not perform electrochemical supercapacitors as well. However, Wang [19] examined these claims and found 208 F/g at 0.4 A/g. The hybrid structure of Fe_3O_4@SiO_2@metal complex nanocomposites has not been studied or reported in any works or research. Through the use of cyclic voltammetry, galvanostatic discharge, and electrochemical impedance spectroscopy, the electrochemical characteristics of the prepared hybrid nanocomposite were examined. The Fe_3O_4@SiO_2@metal complex hybrid nanocompsoite exhibits excellent electrochemical properties, making it a candidate for potential use in supercapacitors.

2. EXPERIMENTAL

2.1 Materials

All of the chemicals, reagents, and solvents used in this work came from Sigma-Aldrich and were used without any purification.

2.2 Synthesis of magnetite Fe_3O_4 nanoparticles

Photolysis was used as a method for producing Fe_3O_4 nanoparticles [20–22]. Nanoparticles were prepared using the 125 W manual irradiation system (Fig. 1). First, 100 ml of distilled water were used to dissolve 1 g of potassium ferricyanide $K_3[Fe(CN)_6]$]. Following that, it was moved to an irradiation system that included a 200 ml beaker that was used as a reactor and was placed in an ice bath to prevent the temperature from rising during the irradiation process. 3ml of 1M NaOH was added while the mixture was being rapidly stirred, and the mixture was then exposed to radiation to produce a black precipitate with magnetic properties. To ensure that all K^+ and CN^- ions were removed, the precipitate was isolated and washed with distilled water once, acetone twice, and ethanol three times. It took 4 hours for it to dry at 80 ºC. The next stage of the preparation processes can now begin with the magnetite precipitate.

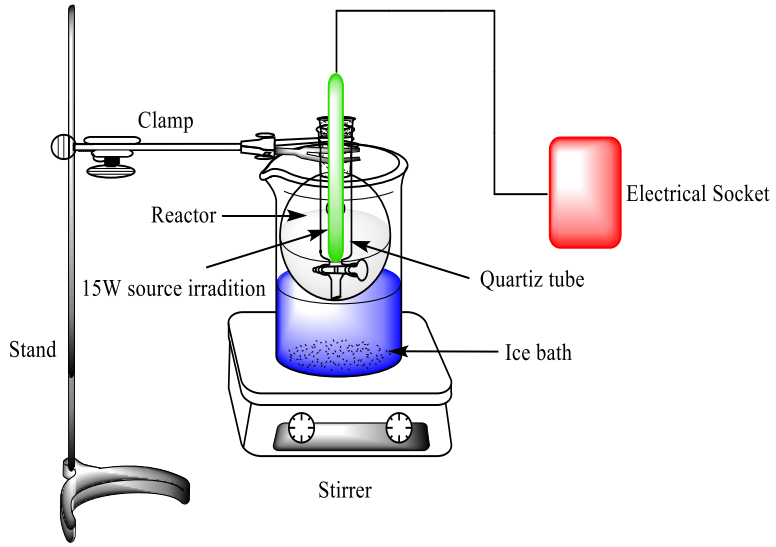

Figure 1. Manual irradiation system

2.3 Preparation of Fe_3O_4@SiO_2-IPTMS

This procedure was broken down into two phases. The first part involved creating the Fe_3O_4@SiO_2 as follows: in a 300 ml beaker, 2g of produced Fe_3O_4 NPs were dispersed in 250 ml of a mixed solution made up of 50 ml of distilled water and 200 ml of propanol for 40 minutes (sol. 1). After that, vigorously stir for 30 minutes at room temperature (35 ºC, July 4, 2022) to create a suspension solution. A second 100 ml beaker containing 2 ml of tetraethyl orthosilicate (TEOS), 20 ml of ethylene glycol (EG), and 5 ml of a 28 percent ammonium solution was used to add to the first beaker's contents under constant stirring for 24 hours at room temperature. After being separated using a powerful magnetic piece, the Fe_3O_4@SiO_2 precipitate was cleaned twice with ethanol and once with distilled water, and it was then dried at 80 ºC. Fe_3O_4@SiO_2-IPTMS was prepared in the second part. 1 g of Fe_3O_4@SiO_2 was dispersed by sonication for 20 minutes in a 250 ml mixture of absolute ethanol and distilled water with a 1:1 ratio under the addition of 3 ml of IPTMS to the suspension. The mixture

was then stirred for the following two hours at room temperature while being bubbled with N2. Before moving on to the next step, the product nanoparticles were isolated by magnetic decantation and dried at 80 ^{o}C.

2.4 Preparation of Fe_3O_4@SiO_2-Cu complex

The final step was broken down into three components, as follows:

1- Preparation of Fe_3O_4@SiO_2-acac: One hour of sonication was used to suspend 1g of Fe_3O_4@SiO_2-IPTMS in 50ml of toluene. Then, with vigorous stirring, an equivalent mole of acetylacetone was added to the suspension. The mixture was then transferred to a round bottom flask with three necks and refluxed for eight hours with a dropper full of NaH under N2 atmosphere conditions. The product was separated by magnetic decantation and repeatedly washed in ethanol and acetone to get rid of the loose materials.

2- Preparation of Fe_3O_4@SiO_2-bis(aminopyridine)

2g of Fe_3O_4@SiO_2-acac were ultrasonically dispersed in 25ml of ethanol to create a suspension solution. The suspension solution of Fe_3O_4@SiO_2-acac was then added, 4g of 2-amino pyridine was dissolved in 25ml of ethanol, and stirred at a reflex process under N2 for 10 hours. To separate the product from the unattached materials, it was isolated using magnetic decantation and repeatedly washed in ethanol. At 80°C, it finally dried.

3- Preparation of Fe_3O_4@SiO_2-bis(aminopyridine)-Cu complex

The final step involved mixing a (2:1) mole ratio of $Cu(NO_3)_2.3H_2O$ and Fe_3O_4@SiO_2-bis (aminopyridine) in 50ml of absolute ethanol, which was then refluxed for 5 hours under nitrogen. By using magnetic decantation to separate the solid product, ethanol was used to wash it repeatedly. At 80 degrees Celsius, it finally dried. All prepared procedures are listed in (Scheme. 1).

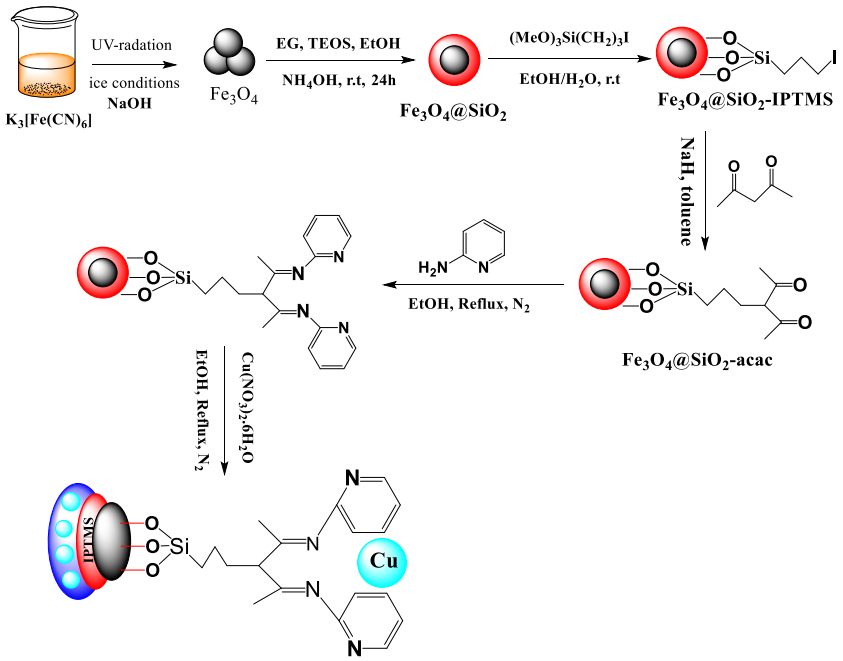

Scheme 1. Prepared of Fe_3O_4@SiO_2-bis(aminopyridine)-Cu complex

3. RESULTS AND DISCUSSION

With the help of FTIR spectroscopy, the structure and functional groups of the prepared materials were identified, and they are depicted in Fig. 2a–e. As seen in Fig. 2a, the Fe3O4 catalyst exhibits a strong adsorption peak that can be attributed to the stretching vibration of the Fe-O bond [23].Two peaks were located at 1077 and 805cm^{-1} (Fig. 2b) characteristic to ν_{as} (Si-O-Si) and ν_s (Si-O-Si) respectively, and a strong peak was centered at 587cm^{-1} back to Fe-O confirming the formation of silica-magnetite shell-core nanoparticles [24].

The dispersed peak of C-I and the appearance of a new adsorption band at 1725 cm^{-1} in the case of Fe3O4@SiO2-acac (Fig. 2d) are characterized by the carbonyl group (C=O) of the acetyl (Fig. 2e). The bonds of pyridine are reflected in a new peak that appears below 1500 cm^{-1}. Following the addition of Cu^{+2} ions, the C-N peaks shifted to a higher wavenumber, indicating that Cu ions and nitrogen successfully combined.

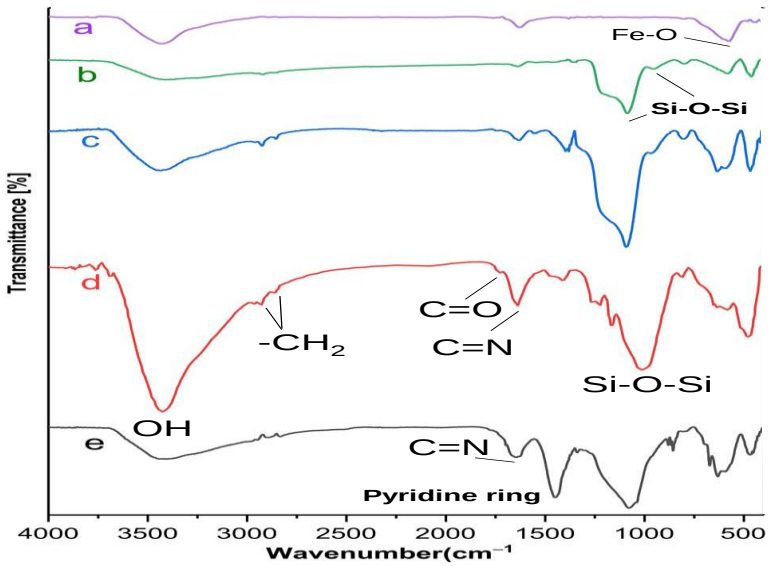

Figure 2. FTIR of (a) Fe_3O_4, (b) Fe_3O_4@SiO_2, (c) Fe_3O_4@SiO_2-IPTMS, (d) Fe_3O_4@SiO_2-acac and (e) Fe_3O_4@SiO_2-bis(aminopyridine)-Cu

The XRD of Fe_3O_4 and Fe3O4@SiO_2-bis(aminopyridine)-Cu is shown in Fig. 3a. Numerous intensity peaks can be seen in the magnetite pattern (Fig. 3) which correspond to the angles of (220), (311), (400), (422), (511) and (440) and these results are consistent with (JCPDS file no. 19-0629). The XRD pattern of Fe3O4@SiO2-bis(aminopyridine)-Cu is shown in Fig. 3. The findings show a strong agreement with the pattern of pared Fe_3O_4 and point to the functionalization process maintaining the crystal structure of magnetite [26]. Additionally, the Fe_3O_4@SiO_2-bis(aminopyridine)-Cu pattern indicates a high degree of dispersion of copper on the nanocomposite, which is not detectable by XRD technique. The copper diffraction peaks cannot be seen in this pattern. The fact that the peak's intensity is waning and shifting to a lower position in Figure 3b, however, provides strong support for the presence of copper ions in the final complex with high dispersion.

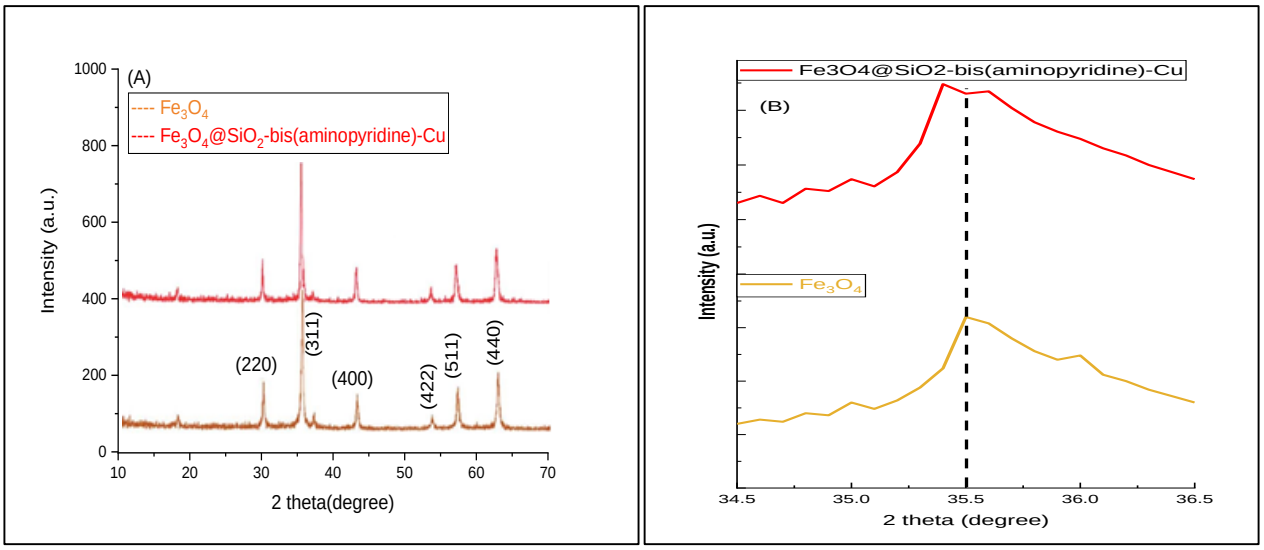

Figure 3. XRD of (A) Fe_3O_4 and Fe_3O_4@SiO_2-bis(aminopyridine)-Cu, (B) deviation (311) peaks

A measurement using X-ray photoelectron microscopy (XPS) was made to look into the oxidation state of the copper ions on the catalyst surface (Fig. 4). The extended spectrum shows two peaks at 953.2 eV and 933.3 eV, which are assigned to $2p_{1/2}$ and $2p_{3/2}$ bonding energies, respectively [27].

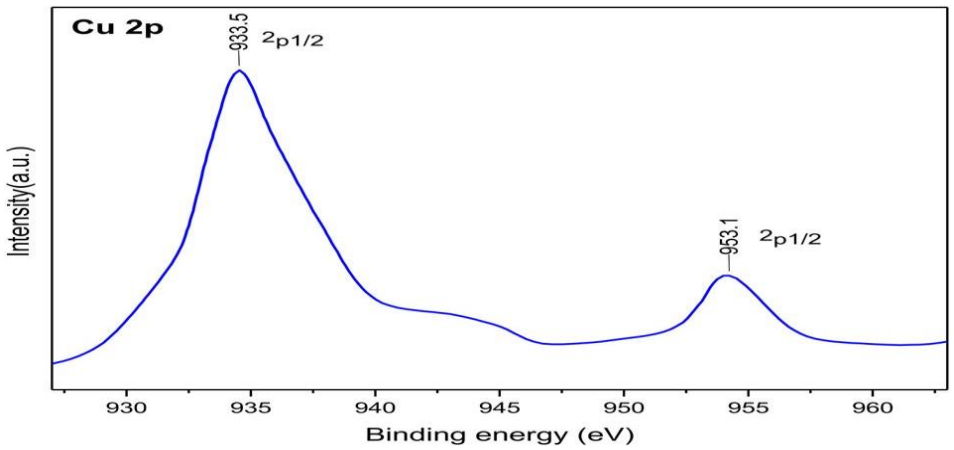

Figure 4. XPS analysis of Fe_3O_4@SiO_2-bis(aminopyridine)-Cu

Fig. 5 illustrates the use of energy dispersive X-ray (EDX) to confirm the presence of Fe, O, Si, C, N, and Cu in the Fe_3O_4@SiO_2-bis(aminopyridine)-Cu. The results show that the covalent adsorption of the ligand (aminopyridine) that took place on the surface of the catalyst was successful because nitrogen atoms (N) are present instead of iodine atoms (I). The outcomes are consistent with those of the XPS analysis, as shown in Fig. 4. Using FESEM mapping analysis, the EDX results were further

justified (Fig. 6). The compositional maps demonstrate the excellent distribution of ion species on the matrix surface, which has a significant impact on the performance of the complex.

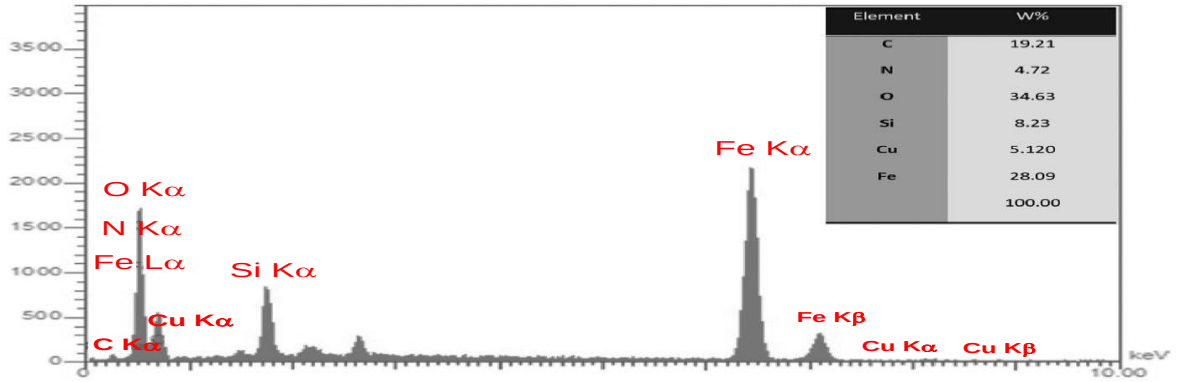

Figure 5. EDX of Fe_3O_4@SiO_2-bis(aminopyridine)-Cu

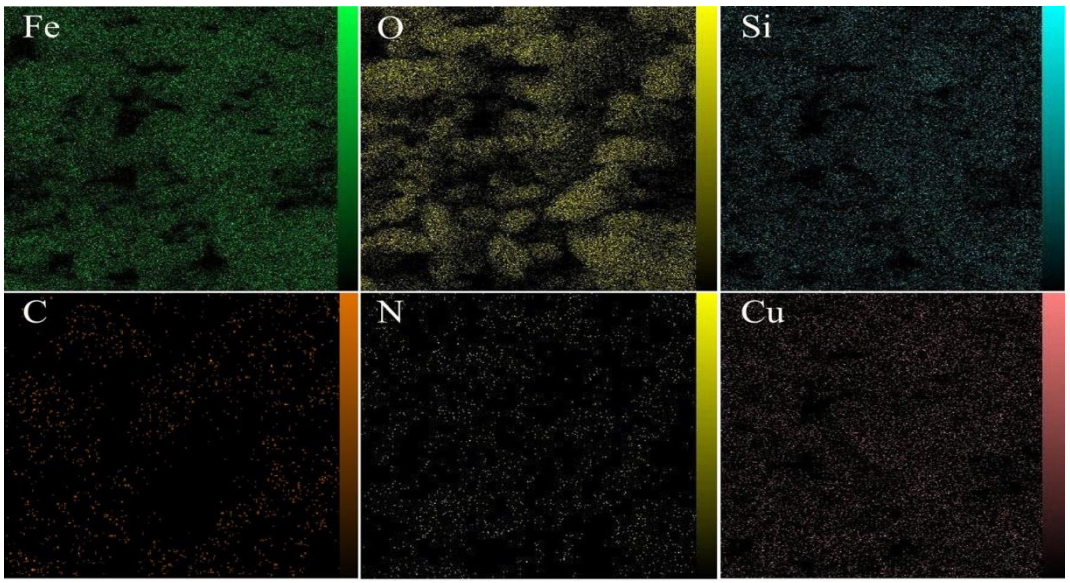

Figure 6. Element mapping of Fe_3O_4@SiO_2-bis(aminopyridine)-Cu

Figs. 7 shows the results of an investigation into the morphology and grain size of Fe_3O_4@SiO_2-bis(aminopyridine)-Cu using transmission electron microscopy (TEM) and scanning electron microscopy (SEM). Results from FESEM images show that there are spherical Fe_3O_4 particles present, and the copper complex is successfully anchored to the catalyst surface. The spherical shapes of the particles may play a major role in preventing accumulation between them and aiding in their even distribution. The TEM images show that synthesized nanoparticles have a spherical morphology with monodispersity and a size range of 17–22 nm; these findings are consistent with those of the FESEM.

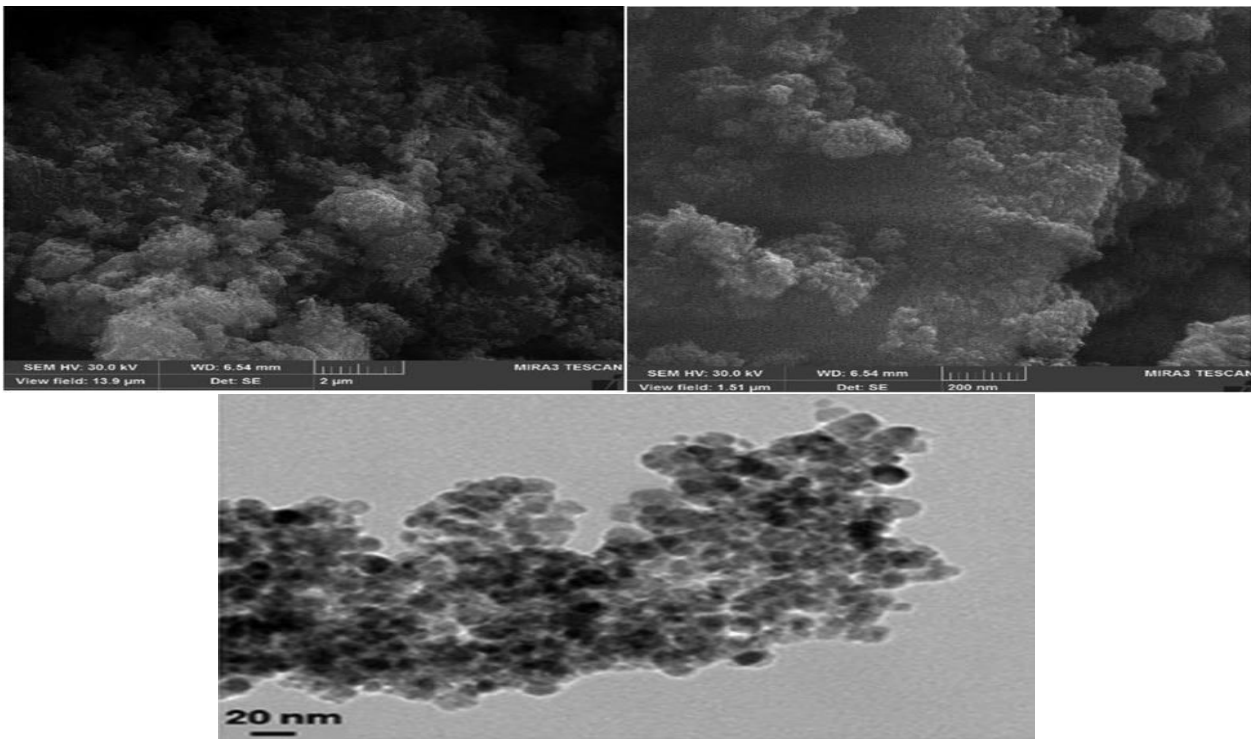

Figure 7. FESEM and TEM of Fe_3O_4@SiO_2-bis(aminopyridine)-Cu

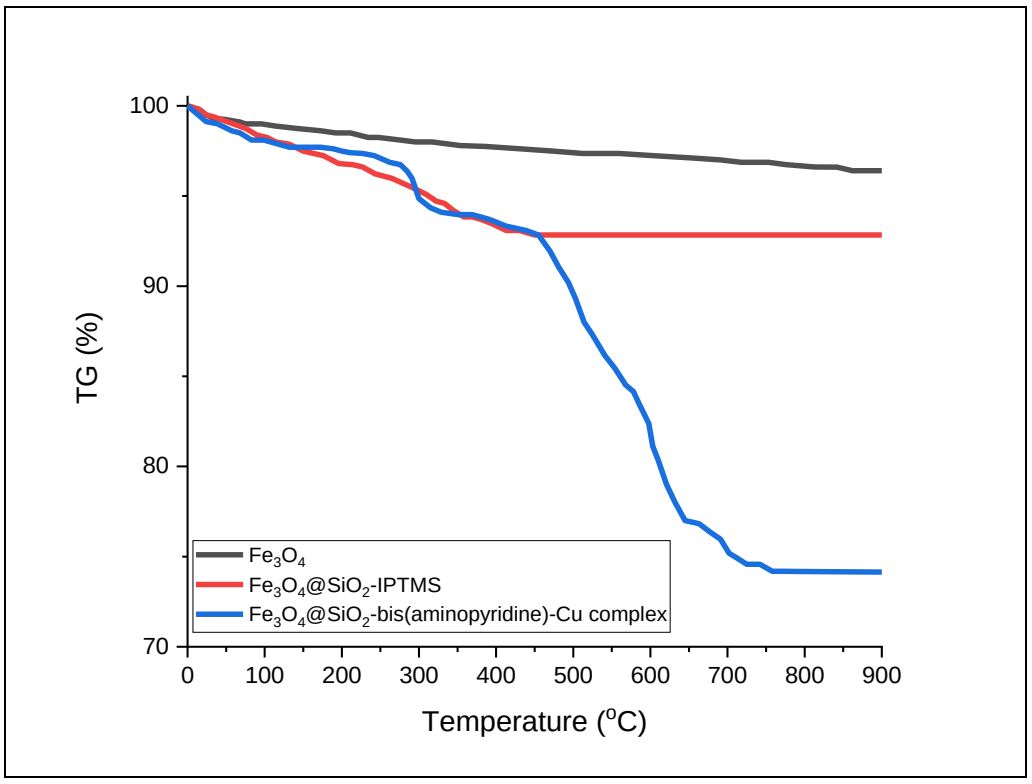

Figure 8. TGA curve of prepared nanomaterials

To evaluate the electrochemical performance of Fe_3O_4 and Fe_3O_4@SiO_2-bis(aminopyridine)-Cu electrodes, the cyclic voltammetry (CV) and chronopotentiometric (CP) analysis were carried out. Fig. 9a-b shows the cyclic voltammogram of Fe_3O_4 and Fe_3O_4@SiO_2-bis(aminopyridine)-Cu electrodes at 10-100mVs^{-1} scan rate and potential rate -0.1-0.6V with different shape and size. Due to the redox reaction occurring at the electrodes as well as the reversible reaction between the ferric/ferrous ions of the electrodes and the electrolyte interface, the curves of the electrodes appear cathodic and anodic peaks back to pseudo-capacitor behavior [30]. Furthermore, the Fe_3O_4@SiO_2-bis(aminopyridine)-Cu electrode has a larger CV area than Fe_3O_4, indicating a higher capacitance, and the peak current of the hybrid nanocomposite is greater than that of pure magnetite, indicating that the SiO2-bis(aminopyridine)-Cu shell enhances the capacitance of Fe3O4.

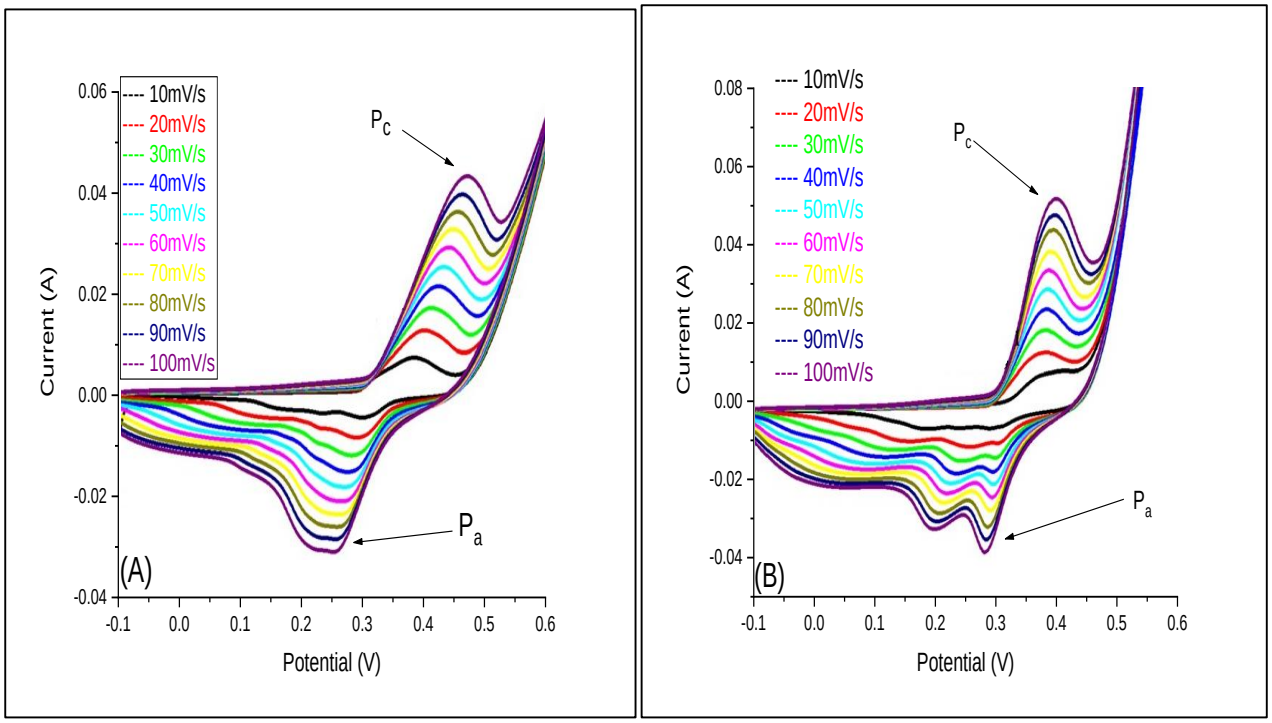

Figure 9. CV curves of (A) Fe_3O_4, (B) Fe_3O_4@SiO_2-bis(aminopyridine)-Cu at different scan rate

At different gravimetric current densities, the discharge curves of Fe_3O_4 and Fe_3O_4@SiO_2-bis(aminopyridine)-Cu were measured in 1M H_2SO_4 and depicted at (Fig. 10 a,b). The specific capacitance of Fe_3O_4 and Fe_3O_4@SiO_2-bis(aminopyridine)-Cu were calculate by using the following equation [31]:

$$Cs = \frac{I\Delta t}{m\Delta E}$$

Where the Cs: specific capacitance, I: current of discharge, Δt discharge time, m: active mass of electrodes, ΔE: IR discharge drops. According to the findings (Fig. 10c), prepared electrodes' specific capacitance appears to decrease as current densities rise, exhibiting pseudocapacitive performance with favorable electrochemical properties. The specific capacitance reduction could be

due to an increase in current, which would reduce the amount of time that ions have to get to or enter the electrodes.

On the other hand, the findings showed that the discharge time is decreasing as the current density is increasing, which assigns to an increase in the drop voltage. The specific capacitance of Fe_3O_4 and Fe_3O_4@SiO_2-bis(aminopyridine)-Cu are 170 and 195A/g, respectively, at the charge current of 10A/g, indicating that the SiO_2-bis(aminopyridine)-Cu shell is increasing the capacitance by supplying a new site for storing energy. Additionally, it offers more options for electron transport on and within Fe_3O_4, and all of these developments have improved electrodes for electrochemical reactions and reduced electrode resistance [32,33].

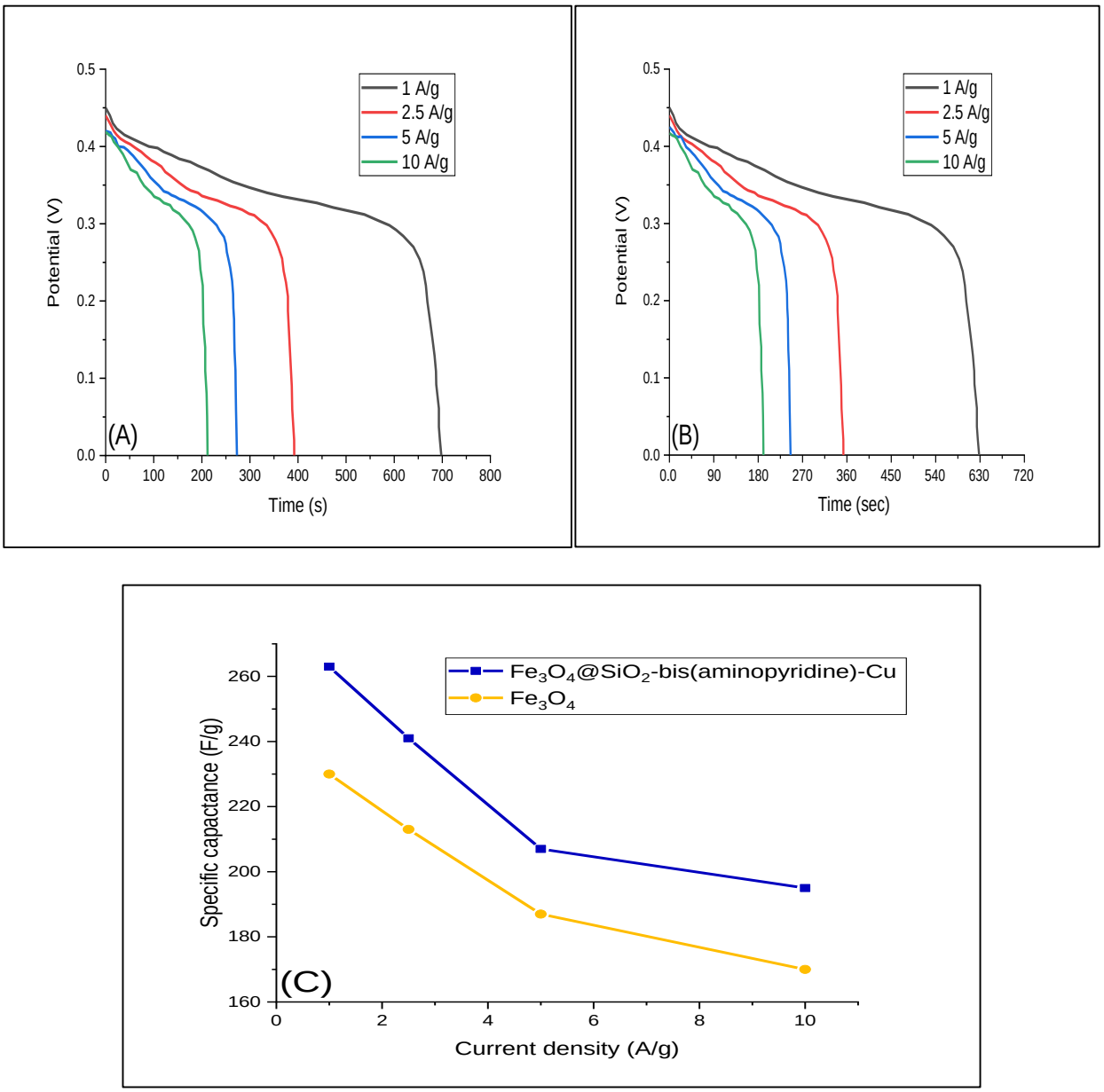

Figure 10. Discharge curve of (A) Fe_3O_4, (B) Fe_3O_4@SiO_2-bis(aminopyridine)-Cu, (C) the relationship of specific capacitance and current density

Measurements of Fe_3O_4 and Fe_3O_4@SiO_2-bis(aminopyridine)-Cu were made using electrochemical impedance spectroscopy in order to assess the interfacial process and investigate rate constant, double layer capacitance, and ionic conductivity. Fig. 11 displays the prepared materials' Nyquist plot, which represents semicircle impedance curves that depend on high and low frequencies. The results showed that the Fe_3O_4 electrode had no semicircles, whereas the Fe_3O_4@ SiO_2-bis(aminopyridine)-Cu electrode had a small semicircle and a charge transfer resistance (Rs 2.18), which indicated that the SiO_2-bis(aminopyridine)-Cu shell improved the electronic conductivity and electronic transfer at the interface electrodes. In light of the findings, it is thought that Fe_3O_4@ SiO_2-bis(aminopyridine)-Cu is superior to Fe_3O_4in terms of prepared power and safety for supercapacitors.

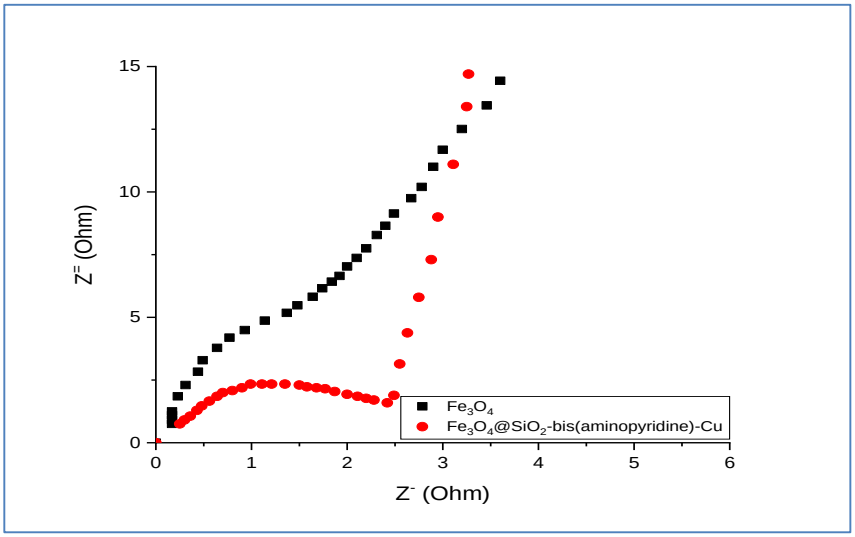

Figure 11. EIS of (A) Fe_3O_4, (B) Fe_3O_4@SiO_2-bis(aminopyridine)-Cu

A 1000 charge-discharge process using 5 A/g and a potential range of 0 to 0.45V was used to examine the cyclic stability of Fe_3O_4 and Fe_3O_4@SiO_2-bis(aminopyridine)-Cu. As can be seen in Fig. 12, Fe_3O_4@SiO_2-bis(aminopyridine)-Cu electrode could still maintain high specific capacitance after cycling after cycling (85%) compare than Fe3O4 electrode (66%), which indicate that the SiO2-bis(aminopyridine)-Cu improve the capactance losing and reversibility of Fe_3O_4 because of the structure of hybrid nanocomposite that does in increasing the synergic interaction between components.

When comparing with other compounds polymeric and oxides compounds (Table. 1), we noted that as-prepared compounds has interesting electrochemical properties between all the previously reported.

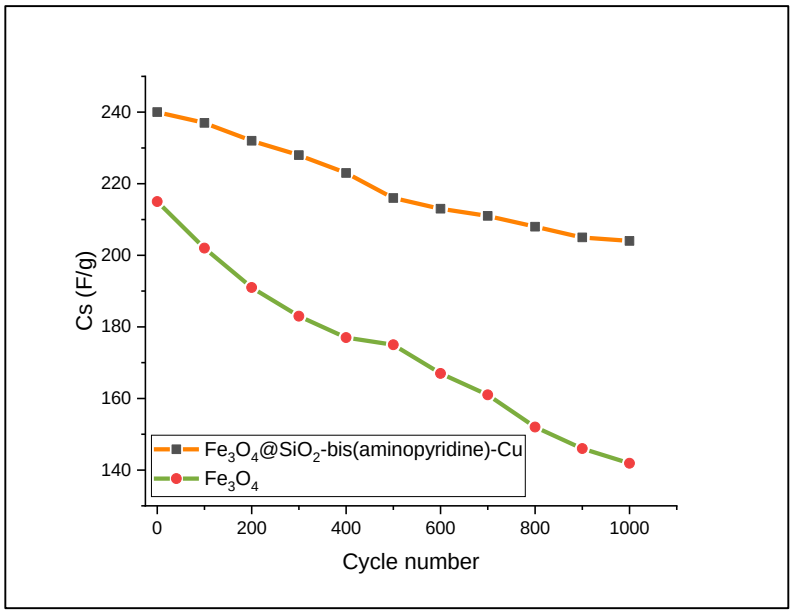

Figure 12. specific capacitance at a constant of 5A/g as a function of cycle number

Table 1. Comparison of specific capacitance of as-prepared compounds with other polymeric and oxides nanocomposite

No.	Compounds	Current density (A/g)	Specific capacitance (F/g)
1	RuO_2/PANI	1	40.2 [34]
2	rGO/PANI		159 [34]
3	Fe_3O_4/C		78 [35]
4	Fe_3O_4@SiO_2-bis(aminopyridine)-Cu		263 [our study]

4. CONCLUSION

In conclusion, the immobilization of bis(aminopyridine)-Cu on the surface of SiO_2-coated Fe_3O_4nanoparticles and photolysis were both successful methods for creating $Fe_3O_4$and Fe_3O_4@ SiO_2-bis(aminopyridine)-Cu nanocomposite. For the described synthesis of oxide nanocomposite, the photolysis approach will be interactive. According to the electrochemical investigation, SiO_2-bis(aminopyridine)-Cu can increase storage energy, enhance the reversibility of Fe_3O_4, and increase specific capacitance. Fe_3O_4@SiO_2-bis(aminopyridine)-Cu nanocomposite is a good electrode for supercapacitor applications because it has a strong retention ratio and specific capacitance as it is currently synthesized.

Reference

1. A. Hodaei, A.S. Dezfuli and H.R. Naderi, *J Mater Sci: Mater Electron*, 29 (2018) 14596.
2. Z.H. Mahmoud, R.A. Al-Bayati and A.A. Khadom, *J. Oleo Sci*., 71 (2022) 311.
3. M. Sobaszek, K. Siuzdak, M. Sawczak, J. Ryl and R. Bogdanowicz, *Thin Solid Films*, 601 (2016)

35.
4. A.A. Al Sarraf, F.H. Alsultany, Z.H. Mahmoud, S.S. Shafik, Z.I. Al and A. Sajjadi, *Synth. Commun*., 52 (2022) 1245.
5. X. Wang, Y. Han, J. Zhang, Z. Li, T. Li, X. Zhao and Y. Wu, *Appl. Radiat. Isot*., 148 (2019) 147.
6. D. Vera, F. Jurado, J. Carpio and S. Kamel, *Energy*, 144 (2018) 41.
7. Z.H. Mahmoud, R.A. Al-Bayati and A.A. Khadom, *Int. J. Electrochem. Sci.*, 16 (2021) 211241.
8. S. Ghasemi and F. Ahmadi, *J Power Sources*, 289 (2015) 129.
9. N. LO, C. Johnston and P.S. Grant PS, *J Power Sources*, 274 (2015) 907
10. Z.H. Mahmood, M. Jarosova, H.H. Kzar, P. Machek, M. Zaidi, A.D. Khalaji, I.H. Khlewee, U.S. Altimari, Y.F. Mustafa and M.M. Kadhim, *JCCS*., 69 (2022) 657.
11. T. Brousse and D. Be´langer, *Electrochem Solid-State Lett*., 6 (2003) 244.
12. H.K. Sharaf, S. Salman, M.H. Abdulateef, R.R Magizov, V.I. Troitskii, Z.H. Mahmoud, R.H. Mukhutdinov and H. Mohanty, *Appl. Phys. A*, 127 (2021) 1.
13. Z.H. Mahmoud, H. Barazandeh, S.M. Mostafavi, K. Ershov, A. Goncharov, A.S Kuznetsov, O.D. Kravchenko and Y. Zhu, *J. Mater. Res. Technol*., 11 (2021) 2015.
14. Z.H. Mahmoud, R.A. AL-Bayati and A.A. Khadom, *Chem. Pap*., 76 (2022) 1401.
15. S.Z. Hussain, M. Ihrar, S.B. Hussain, W.C. Oh and K. Ullah, *SN Appl. Sci.*, 2 (2020) 764.
16. K. Zhang, Y. J. Huang, Y. Xiao, W. Yang, T. Hu, K. Yuan and Y. Chen, *Sci. China Mater*., 63 (2020) 1898.
17. S. Majumder, S. Dey, K. Bagani, S.K. Dey, S. Banerjee, and S. Kumar, *Dalton Trans*., 44 (2015) 7190.
18. G. Wang, L. Zhang and Jiujun Zhang, *Chem. Soc. Rev*., 41 (2012) 797.
19. L. Wang, H. Ji, S. Wang, L. Kong, X. Jiang and G. Yang, *Nanoscale*, 5 (2013) 3793.
20. Z.H. Mahmoud, M.S. Falih, O.E. Khalaf, M.A. Farhan and F.K. Ali, *J Adv Pharm Edu Res*., 8 (2018), 51.
21. Z.H. Mahmoud, R.A. AL-Bayati, A.A. Khadom, *Mater. Today*, 61 (2022) 799.
22. Z.H. Mahmoud, R.A. AL-Bayati and A.A. Khadom, *J Mater Sci: Mater Electron*, 33 (2022) 5009.
23. M.M. Ba-Abbad, A. Benamour, D. Ewis, A. Mohammad and E. Mahmoudi, *JOM*., 23 (2022) 5673.
24. R. Dawn, M. Zzaman, F. Faizal, F.C. Kiran, A. Kumari, R. Shahid, C. Panatarani, I. M. Joni, V. K. Verma, S.K. Sahoo, K. Amemiya and V.R. Sing, *Braz J Phys*., 52 (2022) 99.
25. N. Fatima, S. Nisar and S. Z. Abbas, *ECB*., 9, (2020) 119.
26. Z. Lv, Q. Wang, Y. Bin, L. Huang, R. Zhang, P. Zhang and M. Matsuo, *J. Phys. Chem. C*, 119 (2015) 26128.
27. M.S. Pourbavarsad, B.J. Jalalieh, C. Harkins, R. Sevanthi and W.A. Jackson, *J. Environ. Chem. Eng*., 9 (2021) 106271.
28. X. Tan, P. Sudarsanam, J. Tan, A. Wang, H. Zhang, H. Li and Song Yang, *J. Environ. Chem. Eng*., 9 (2021) 104719.
29. J. Safaei-Ghomi, F. Eshteghal and H. Shahbazi-Alavi, *J. Iran. Chem. Soc*., 15 (2018) 661.
30. V.P. Joshi, N. Kumar and R.R. Salunkhe, *Springer, Cham*., 34 (2021) 601.
31. C. Lai, Y. Guo, H. Zhao, H. Song, X. Qu, M. Huang, S.W. Hong and K. Lee, *Adv Compos Hybrid Mater*, 32 (2022) 12.
32. K.S. Lee, Y.J. Seo, and H.T. Jeong, *Carbon Lett*., 31 (2021) 1041.
33. R. Balamurugan, S.S. Shalini and A.C. Bose, *J Mater Sci: Mater Electron*, 33, (2022) 18231.
34. M. Ates and M. Yildirim, *Polym Bull*, 77 (2020) 2285.
35. S.K. Park, J. Sure D. Vishnu, S.J. Jo, Lee, W.C. Ahmed Kim I.A. and H.K. Kim, *Energies*, 14 (2021) 2908.